ACS APPLIED MATERIALS & INTERFACES

Research Article

www.acsami.org

# Tuning Gelation Kinetics and Mechanical Rigidity of β-Hairpin Peptide Hydrogels via Hydrophobic Amino Acid Substitutions

Cuixia Chen,[†] Yanfeng Gu,[†] Li Deng,[†] Shuyi Han,[†] Xing Sun,[†] Yucan Chen,[†] Jian R. Lu,[‡] and Hai Xu*[,†]

[†]State Key Laboratory of Heavy Oil Processing and the Centre for Bioengineering and Biotechnology, China University of Petroleum (East China), 66 Changjiang West Road, Qingdao, Shandong 266580, China

[‡]Biological Physics Laboratory, School of Physics and Astronomy, University of Manchester, Schuster Building, Manchester M13 9PL, United Kingdom

Supporting Information

**ABSTRACT:** Self-assembling peptide hydrogels with faster gelation kinetics and higher mechanical rigidity are favorable for their practical applications. A design strategy to control the folding, self-assembly, and hydrogelation of β-hairpin peptides via hydrophobic amino acid substitutions has been explored in this study. Isoleucine has higher hydrophobicity and stronger propensity for β-sheet hydrogen bonding than valine. After the valine residues of MAX1 (VKVKVKVKV$^{D}$PPTKVKVKVKV-$NH_2$) were replaced with isoleucines, oscillatory rheometry and circular dichroism (CD) spectroscopy characterizations indicated that the variants had clearly faster self-assembly and hydrogelation rates and that the resulting gels displayed higher mechanical stiffness. Transmission electron microscopy (TEM) indicated the parent MAX1 and its variants all formed networks of long and entangled fibrils with the similar diameters of ∼3 nm, suggesting little effect of hydrophobic substitutions on the self-assembled morphology. The MAX1I8 (IKIKIKIKV$^{D}$PPTKIKIKIKI-$NH_2$) hydrogel showed the fastest gelation rate (within 5 min) and the highest gel rigidity with the series, supporting the homogeneous cell distribution within its 3D scaffold. In addition, the MAX1I8 hydrogel showed quick shear-thinning and rapid recovery upon cessation of shear strain, and the MTT and immunological assays indicated its low cytotoxicity and good biocompatibility. These features are highly attractive for its widespread use in 3D cell culturing and regenerative medical treatments.

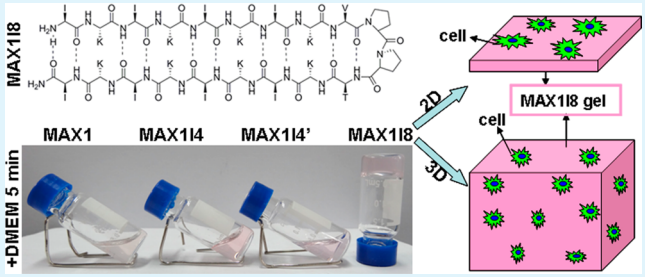


**KEYWORDS:** *peptide hydrogel, β-hairpin peptide, residue substitution, gelation kinetics, gel rigidity, biomedical scaffold*

## 1. INTRODUCTION

Molecular self-assembly based on noncovalent interactions represents a promising strategy for the preparation of advanced materials.[1,2] It connects the relative simplicity of constituent molecules to the complexity of macroscopic materials formed. Thus, by careful molecular engineering of the building blocks, the ultimate material characteristics such as morphology, structure, physiochemical property, and functions can be controlled at the molecular level. Due to the inherent biocompatibility and biochemical properties of peptides, their self-assembly has attracted considerable attention, and the resulting materials have shown great potential in a wide range of biotechnological and biomedical applications.[2−20] In addition, the sequence and structural diversity of peptides as well as their easy and commercial accessibility via standard solid phase synthesis protocols are stimulating research in this area.

Self-assembling peptide hydrogels are of particular interest as an emerging class of functional biomaterials for biomedical applications. Several recent reviews have summarized self-assembling peptides and peptide derivatives capable of forming hydrogels that can serve as 2D and 3D biological scaffolds and injectable drug delivery matrices.[21−25] Distinct from conventional hydrogels derived from high molecular weight natural and synthetic polymers, the peptide hydrogels take advantage of the self-assembly of small molecular weight peptides, thus minimizing the risk of biological and chemical contaminations during macromolecular separation and synthesis. Other possible advantages of self-assembling peptide hydrogels include their biocompatibility, biodegradability, structural resemblance to natural extracellular matrices, and responsiveness to environmental stimuli.

For practical uses, however, several criteria still have to be addressed for these peptide-based hydrogels. Their gelation kinetics and the final mechanical rigidity are of critical importance, because these properties have profound impacts on cell distributions within scaffolds and subsequent cell fates.[22,26−30] Furthermore, scaffolds with higher stiffness are always more favorable for practical handling and changes of medium.[22,31] To date, enhancing mechanical properties of self-assembling peptide hydrogels is still challenging, although several methods have been explored, including covalent cross-linking via native chemical ligation,[31] disulfide bond for-

Received: June 9, 2014
Accepted: August 4, 2014
Published: August 4, 2014

 © 2014 American Chemical Society 

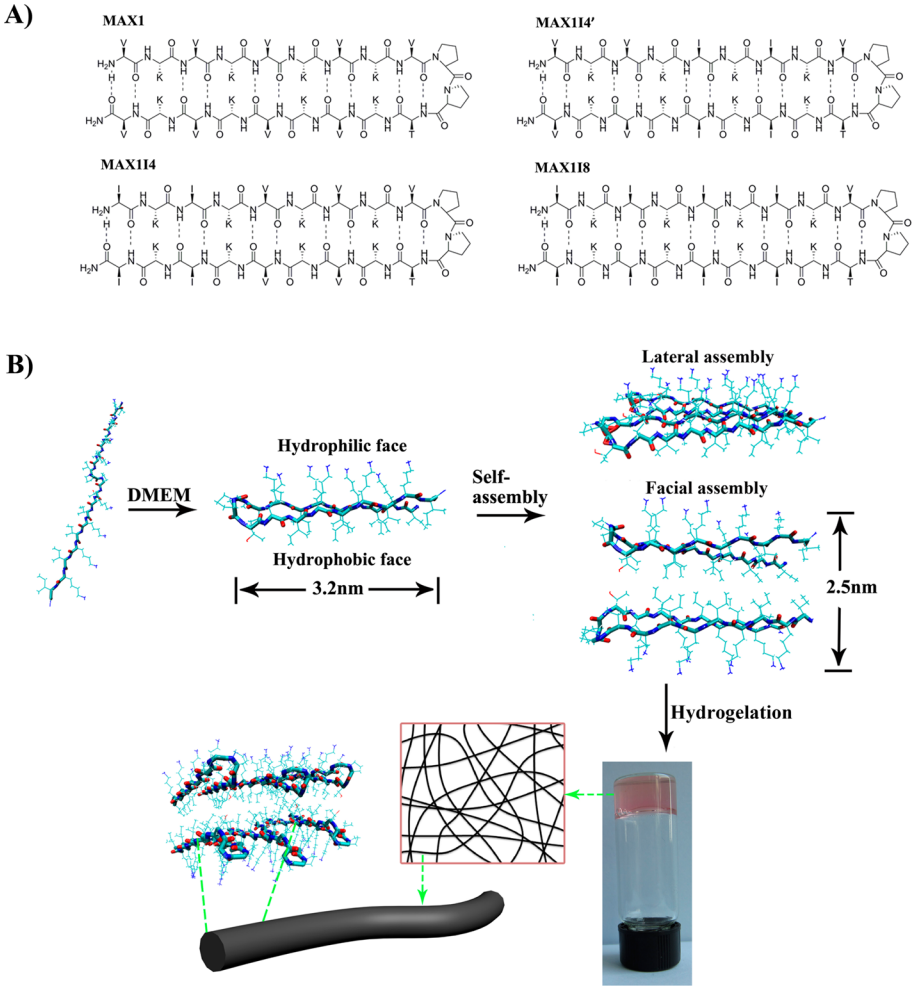


**Figure 1.** A) Folded hairpin structures of MAX1, MAX1I4, MAX1I4′, and MAX1I8 peptides. B) Schematic self-assembly process of MAX1I8 peptide.

mation,[32,33] and enzymatic chemistry,[34] ion complexation (e.g., borate, phosphate, magnesium, and zinc ions),[32,35,36] and even mixing of enantiomers.[37] On the other hand, because of the diverse properties (e.g., hydrophobicity, aromaticity, geometry, charge and isoelectric point) of the different amino acids in combination with their propensities for forming certain conformations (e.g., $\beta$-sheet and $\alpha$-helix), it is also feasible to enhance the mechanical rigidity of peptide gels via residue and sequence modifications.[30,38−40]

As an typical example of the well-studied self-assembling peptides, the sequence of MAX1 (VKVKVKVKV$^{D}$P-PTKVKVKVKV-$NH_2$) developed by Pochan and Schneider et al. is a 20-residue peptide, consisting of a type II′ $\beta$-turn (-V$^{D}$PPT-) that is flanked by N- and C-terminal extended strands of alternating hydrophobic valine and hydrophilic lysine residues.[41,42] The peptide is unfolded in low ionic strength buffer at pH 7.4 due to electrostatic repulsion between protonated lysine side chains. The lysine-based charge interaction can be alleviated via deprotonation at higher pH or charge screening with salts at physiological pH (7.4), thus allowing the peptide to undergo intramolecular folding into an facially amphiphilic $\beta$-hairpin, with all valine residues on one face of the hairpin with lysine residues on the other. Once folded, the peptide molecules subsequently undergo self-assembly to form a fibrillar gel network, driven by intermolecular interactions such as lateral $\beta$-sheet hydrogen bonding, side chain-side chain hydrophobic contacts and facial hydrophobic collapse. To increase the gel rigidity, most research on this kind of $\beta$-hairpin peptides has focused on the hydrophilic amino acid residues on the two flanking strands, including borate ion complexation and a point substitution for positively charged lysine with negatively charged glutamic acid or uncharged threonine.[30,35,38,39] In contrast, less attention has been paid to the hydrophobic amino acid residues, although the intra- and intermolecular hydrophobic interactions also play important roles in the peptide folding and subsequent self-assembly of hairpins.[43,44]

In this paper, we have designed and synthesized three variants based on MAX1 by partly or completely replacing hydrophobic valine residues with isoleucines, i.e. IKIKVKVK-V$^{D}$PPTKVKVKIKI-$NH_2$, VKVKIKIKV$^{D}$PPTKIKIKVKV-$NH_2$, IKIKIKIKV$^{D}$PPTKIKIKIKI-$NH_2$, denoted as MAX1I4, MAX1I4′, and MAX1I8, respectively (Figure 1A). Because isoleucine is more hydrophobic and has a higher $\beta$-sheet forming propensity than valine,[45,46] such substitutions are expected to accelerate the self-assembly and hydrogelation kinetics, finally producing hydrogels with increased stiffness. We have studied these effects with time using oscillatory rheometry and circular dichroism (CD) spectroscopy. Transmission electron microscopy (TEM) has been used to characterize the gel microstructure. We have also assessed the cell cytotoxicity and biocompatibility of the peptide gel by using


dx.doi.org/10.1021/am5036303 | ACS Appl. Mater. Interfaces 2014, 6, 14360−14368

the MTT and immunological assays. The cell distribution within the gel scaffold has been observed by using laser confocal microscopy.

## 2. EXPERIMENTAL SECTION

**Materials.** The materials for peptide synthesis including Fmoc-protected amino acids, O-(1*H*-benzotriazole-1-yl)-*N*,*N*,*N*′,*N*′-tetramethyluronium hexafluorophosphate (HBTU), *N*-hydroxybenzotriazole anhydrous (HOBT), *N*,*N*′-diisopropyl ethylamine (DIEA), trifluoroacetic acid (TFA), triisopropylsilane (TIS), and Rink amide-MBHA resin were purchased from GL Biochem Ltd. (Shanghai) and used as received. Piperidine, dichloromethane (DCM), and *N*,*N*′-dimethylformamide (DMF) were purchased from Bo Maijie Technology (Beijing) and were redistilled prior to use. Calcein acetoxymethyl ester (calcein-AM), 3-(4,5-dimethylthiazol-2-yl)-2,5-diphenyltetrazolium bromide (MTT), and other chemicals were obtained from Sigma (St. Louis, MO) and used as received. Water used in all experiments was processed with a Millipore Milli-Q system (18.2 MΩ·cm).

Mouse embryonic fibroblast NIH 3T3 cells and human embryonic kidney HEK 293 cells were obtained from the Cell Bank in Shanghai Institute of Cell Biology. Cells were cultured in DMEM (Dulbecco's modified Eagle's medium, pH 7.4) with 10% fetal bovine serum (FBS) at 37 °C under 5% $CO_2$.

**Peptide Synthesis and Gel Preparation.** The peptides were synthesized using Fmoc solid-phase synthesis strategy on a CEM Liberty microwave peptide synthesizer. Note that the use of Rink amide resin allowed their C-termini to be amidated, while their N-termini were uncapped. Detailed synthesis and purification procedures have been described in our previous work.[15] The final products were subjected to MS (MALDI-TOF) and HPLC analyses, indicating their high purity (>98%).

The synthesized peptides were dissolved in 25 mM Hepes (pH 7.4) to obtain the peptide solutions with a concentration of 4 wt %. To trigger peptide folding and subsequent self-assembly and hydrogelation, an equal volume of DMEM was added and gently mixed at room temperature (20 ± 2 °C).

**CD Spectroscopy.** CD spectra were recorded on a Biologic Mos-450/AF-CD spectrophotometer at room temperature (20 ± 2 °C) using a 0.1 mm quartz cell. The wavelength scans were performed between 190 and 250 nm with a 0.5 nm step. The CD signals presented were the average of six individual measurements for each sample, expressed as $[\theta]$ (deg·cm$^2$/dmol).

**Rheology.** Dynamic time and frequency sweep measurements were performed on a Thermo Scientific Haake MARS III modular rheometer operating in a cone−plate mode (cone angle: 2.0°, diameter: 34.995 mm, truncation: 0.105 mm) at 25 °C. The temperature was controlled by a Peltier temperature module for cones and templates. During rheological measurements, the cone−plate cell was covered with a solvent trap to prevent water evaporation. Strain sweeps were first conducted to determine the linear viscoelastic regime, in which all the following rheological measurements were performed. Dynamic time sweep measurements were performed at a frequency and strain of 6.28 rad/s (1 Hz) and 1%, respectively. Dynamic frequency sweep measurements were performed with a frequency and strain of 0.1−100 rad/s and 1%, respectively. For the shear-thinning experiment, a dynamic time sweep (6.28 rad/s and 1% strain) was performed for 5 min after loading a gel, followed by the application of 1000% strain for 2 min to shear-thin the gel. Then, the strain was decreased to 1%, and the dynamic time sweep was performed again. Such a shear-thin and recovery cycle was performed twice.

**TEM.** TEM micrographs were obtained on a JEOL JEM-2100 UHR electron microscope operated at an accelerating voltage of 200 kV. For the sample preparation, a drop of peptide hydrogel was delivered on a glass slide through syringe. Following short contact with the gel, a 300-mesh copper grid was negatively stained with 2% uranyl acetate aqueous solution for 3 min, and excess solution was then removed with a filter paper.

**Cell Attachment, Proliferation, and Biocompatibility.** To produce a gel for 2D cell culture, 150 μL of the resulting 2 wt % MAX1I8 peptide solution was added into a 48-well tissue culture polystyrene (TCPS) plate immediately after mixing DMEM with 4 wt % MAX1I8 solution with an equal volume. After gelation for 4 h, cells ($5 \times 10^5$ cells/mL, 150 μL) were plated on the formed gel and incubated in DMEM with 10% fetal bovine serum (FBS) at 37 °C under 5% $CO_2$. The cells seeded in the wells without the peptide gel served as the control. The culture medium was refreshed every 24 h.

To test cell viability and proliferation, the MTT assay was performed. Briefly, after incubation for the indicated times, 20 μL of MTT solution (5 mg/mL) was added to each well, and the cells were incubated for further 4 h at 37 °C. The precipitated formazan was dissolved in 200 μL of dimethyl sulfoxide. The absorbance at 570 nm ($A_{570}$) was measured using a microplate autoreader (Molecular Devices, M$^2$e). Note that the gel coated wells without cells acted as the blank for those with cells during the $A_{570}$ measurement.

To more clearly observe cell attachment and spread, the seeded cells on the gel were stained with calcein-AM. Briefly, the medium was removed from the wells, and the cells were washed with DMEM for three times. Then, the cells were stained with 1 μM calcein-AM (100 μL) for 30 min at room temperature, followed by removing the dye solution and washing with PBS for three times. Finally, the cells were observed using a laser confocal microscope (Nikon AI-si).

To test the gel biocompatibility, human lymphocytes were isolated from whole blood cells by the standard Ficoll method, and an immunological assay was then performed.[47] Briefly, 10 mL of blood obtained from healthy volunteers was diluted with 10 mL PBS and was carefully added to a Ficoll solution of 1.077g/mL with the ratio of Ficoll to blood at 2:1. The resulting solution was centrifuged at 2000 rpm for 15 min. The ring with lymphocytes was harvested. The collected lymphocytes were washed with PBS for three times and suspended in DMEM for use. 200 μL of 2 wt % MAX1I8 hydrogel was injected into a 24 well TCPS plate, and 200 μL of lymphocytes in DMEM ($2 \times 10^6$ cells/mL) was seeded on the forming hydrogel surface. After incubation for 1 h at 37 °C under 5% $CO_2$, the lymphocytes were collected and washed for three times. Total RNA from the lymphocytes was extracted by Trizol (Invitrogen, UK) and 1 μg of RNA was subject to cDNA synthesis with random primers (PrimeScript Reverse Transcriptase, Takara, Japan). Transcriptional levels of TNF$\alpha$, IL8, and $\beta$-actin genes were first tested by RT-PCR (real-time PCR) with a 7500 real-time PCR system (Applied Biosystems, American). The data were analyzed by the relative quantitation of $2^{-\Delta\Delta Ct}$ method.[48] The following primers were used: $\beta$-actin sense, 5′-ATGCCAGGGTACATGGTGGT-3′; antisense, 5′-TCGTGCGTGACATTAAGGAG-3′; IL8 sense, 5′-CGGAAGGA-ACCATCTCACTGTG-3′; antisense, 5′-AGAAATCAGGAAGGC-TGCCAAG-3′; TNF$\alpha$ sense, 5′-CGGGACGTGGAGCTGGCCGA-GGAG-3′; TNF$\alpha$ antisense, 5′-CACCAGCTGGTTATCTCTCA-GCTC-3′. To further understand the TNF$\alpha$ and IL8 expression, we then tested the secretions of the two cytokines by lymphocytes on the gel by using ELISA as previously reported.[49] Note that the incubation of lymphocytes for ELISA lasted for 48 h at 37 °C under 5% $CO_2$. The lymphocytes seeded in the TCPS wells without the gel served as the negative control. For lipopolysaccharide (LPS) induced lymphocytes activation (the positive control), LPS at a final concentration of 2 μg/mL was added into the wells with lymphocytes.

**Cell Distribution within the 3D Gel Scaffold.** NIH3T3 cells were prelabeled with calcein-AM (2 μM) in DMEM for 45 min, washed with DMEM for three times, and resuspended in DMEM at a concentration of $5 \times 10^6$ cells/mL. 100 μL of the cell suspension was added into an Eppendorf tube containing 100 μL of 4 wt % peptide solution in 25 mM Hepes, and then the mixture was immediately transferred into an 8-well borosilicate confocal plate. The cell distribution within the gel scaffold was observed by using ×10 magnification on a laser confocal microscope (Nikon AI-si).

## 3. RESULTS

**Hydrogel Formation.** The peptides were dissolved in 25 mM Hepes (pH 7.4) at a concentration of 4 wt %. They were unfolded at such relatively low ionic strength. Their solutions were freely flowing with little change in viscosity from the buffer. To initiate peptide structural folding, an equal volume of DMEM medium (pH 7.4) was added (Figure 1A). DMEM has a high salt content (around 165 mM) and has been used to trigger the folding, self-assembly, and gelation of hairpin peptides, due to the effective electrostatic screening of their lysine side chain charges.[30,42,50] In addition, DMEM can provide nutrients for cell growth. These features make it advantageous for the use of peptides as scaffolds for cell growth and other types of biomaterial applications including biosensors and medical implants.

After mixing the two solutions, we immediately observed gelation at room temperature (20 ± 2 °C) (Figure 2B-D).

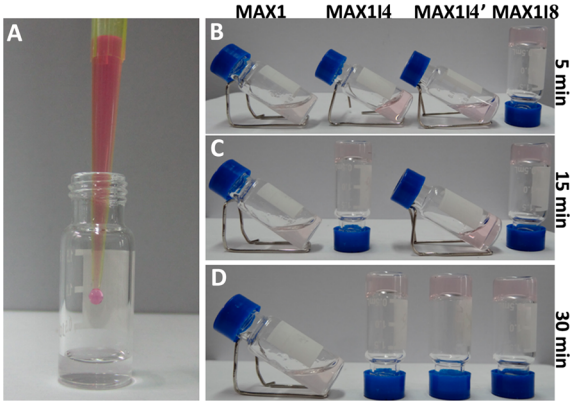


**Figure 2.** Gelation processes of MAX1, MAX1I4, MAX1I4′, and MAX1I8 at room temperature (20 ± 2 °C) with time: A) 0 min, B) 5 min, C) 15 min, and D) 30 min. The gelation was triggered by adding an equal volume of DMEM (pH 7.4) into 4 wt % peptide solutions (25 mM Hepes, pH 7.4).

MAX1I8 formed a clear and self-supporting gel within 5 min after the addition of DMEM (Figure 2B), while the other peptide solutions remained freely flowing within this period. MAX1I4 and MAX1I4′ required 15 and 30 min to form self-supporting gels, respectively (Figure 2C). For the parent MAX1, a self-supporting gel was achieved after ∼1.5 h. The time dependent processes suggest that substitutions of isoleucine residues for valines can accelerate the hydrogel formation kinetics. Furthermore, the kinetic acceleration is not only dependent on the number but also the exact position of residue substitutions within the peptide sequence.

**Rheological Properties.** The differences in hydrogel formation kinetics were further assessed by using time sweep rheology, from which the evolution of storage moduli ($G'$) was measured as a function of time at 25 °C (Figure 3A). $G'$ reflects the mechanical rigidity of gels, and a $G'$ of 100 Pa is believed to be sufficient to support cells within 3D scaffolds.[30] MAX1 underwent gelation very slowly, and it required around 75 min to realize a $G'$ of 100 Pa at this temperature. After valine residues were replaced with isoleucines, the variants showed faster gelation rates. For example, MAX1I8, containing eight substituted isoleucine residues, displayed the fastest gelation rate under the same conditions, with its $G'$ exceeding 100 Pa within the first 30 s. Furthermore, a $G'$ of 1320 Pa was attained after 2 h of gelation, and the gel continued to stiffen afterward (Figure 3A). MAX1I4 and MAX1I4′, in which only four valine residues were replaced, formed gels at rates intermediate to MAX1 and MAX1I8. However, MAX1I4 underwent gelation much more quickly than MAX1I4′. The former attained a $G'$ of 100 Pa within 10 min, while the latter achieved such a $G'$ value after around 30 min. It was evident that for the same number of substitutions, the hydrophobic substitution made close to the central tetrapeptide (-V$^{D}$PPT-) disfavored gelation. This can be interpreted as occurrence of significant steric effect upon intramolecular folding. On the other hand, different locations of substitution may well affect the amphiphilicity of the peptides, altering their propensity for intermolecular assembly.

After 4 h of hydrogelation, $G'$ tended to equilibrated values for the four peptide solutions (2 wt %). Figure 3B shows their frequency sweeps from 0.01 to 100 rad/s at 1% strain in the linear viscoelastic region. Fast hydrogelation kinetics clearly led to gels with higher rigidity, consistent with previous studies, possibly as a result of more cross-links formed.[12,30,38] The equilibrated $G'$ values for MAX1, MAX1I4, MAX1I4′, and MAX1I8 were 373, 492, 942, and 1494 Pa at 6.28 rad/s (1 Hz). Furthermore, the $G'$ values exceeded their corresponding loss moduli ($G''$) by 1 order of magnitude for all the peptide solutions. There was no crossing of $G'$ and $G''$, and both moduli were relatively constant over the measured frequency range. These observations suggest that these peptide solutions have formed rigid and solid-like hydrogels with significant cross-linked networks.

Due to their wide-ranging gelation kinetics and mechanical properties, these hydrogels have potential for many biotechnological applications in cell culturing, tissue engineering, and drug delivery. To use them as injectable materials, the peptide

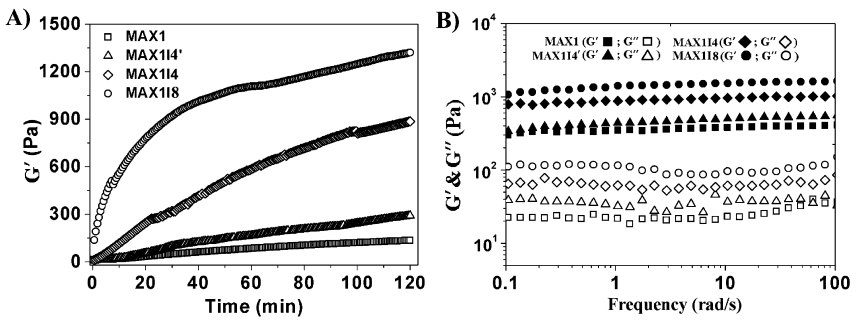


**Figure 3.** A) Storage moduli ($G'$) of 2 wt % MAX1, MAX1I4, MAX1I4′, and MAX1I8 at 25 °C as a function of time. Hydrogel formation was triggered by mixing an equal volume of DMEM with 4 wt % peptide solutions (25 mM Hepes, pH 7.4). B) Dynamic frequency sweeps (1% strain) of 2 wt % MAX1, MAX1I4, MAX1I4′, and MAX1I8 at 25 °C after 4 h of hydrogelation.


dx.doi.org/10.1021/am5036303 | ACS Appl. Mater. Interfaces 2014, 6, 14360−14368

hydrogels should be able to undergo shear thinning with rapid recovery in addition to the above characteristics. To demonstrate this, we applied 1000% strain to the MAX1I8 gel for 2 min. As shown in Figure 4, 1000% strain converted instantly the gel into a liquid ($G' < 10$ Pa). Upon cessation of shear, the gel recovered with a faster kinetics than the initial hydrogelation process (Figure 3A). When such a cycle was repeated, the recovery kinetics of the gel showed a further increase and $G'$ attained a higher value of around 1640 Pa at 30 min after cessation of shear. The quick recovery suggests that the gel's nanostructures and most of the noncovalent cross-links remained intact during shear-thinning. The application of strain was most likely to only disrupt some of the physical connections between gel domains, leading to limited deformation of the macroscopic structures. Furthermore, the MAX1I8 hydrogel recovered rapidly and kept intact on a vertically positioned glass slide after syringe delivery (inset, Figure S1 in the Supporting Information). The quick shear-thinning and recovery property make the MAX1I8 hydrogel very useful for the delivery of cells or drugs to wound sites by syringe in regenerative surgery.

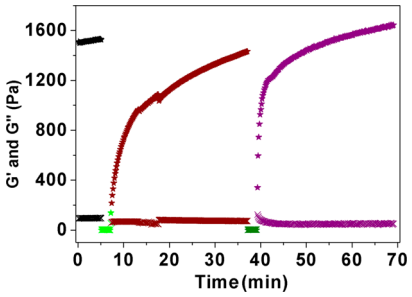


**Figure 4.** Recovery kinetics of the MAX1I8 hydrogel at 25 °C. After loading the gel, $G'$ (stars) and $G''$ (crosses) were monitored for 5 min at a frequency and strain of 6.28 rad/s and 1%, respectively, followed by the application of 1000% strain for 2 min. Then the strain was decreased to 1%, and the dynamic time sweep was performed for 30 min. Such a shear-thinning and recovery cycle was repeated as indicated by different coloring schemes.

**Secondary Structure and Microstructure.** Before the addition of DMEM, all peptides displayed CD signals characteristic of random coil conformation. However, they transformed into $\beta$-sheet conformation after the addition of DMEM. At 2 wt % of peptides, it typically took about 1 min for the transforming processes to complete, suggesting rather rapid folding and $\beta$-sheet structuring relative to the subsequent gelation. Because the formation of $\beta$-sheets is concentration dependent for this kind of hairpin peptides,[41] we also examined the dynamic $\beta$-sheet forming processes at a peptide concentration to 0.5 wt % via CD spectroscopy (Figure 6).

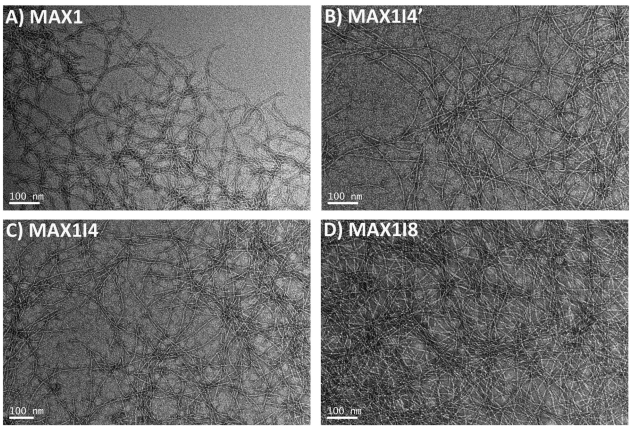


**Figure 6.** TEM images of 2 wt % peptide hydrogels: A) MAX1, B) MAX1I4′, C) MAX1I4, and D) MAX1I8.

MAX1I8 could still adopt the typical $\beta$-sheet conformation about 1 min after the addition of DMEM, with a minimum at ~216 nm, and there was little change in the negative peak's position and intensity after 60 min. In contrast, MAX1 adopted predominantly random coil secondary structure at 1 min, with a minimum at ~200 nm. After 60 min, this minimum position shifted to ~210 nm, indicating a mixture of $\beta$-sheet and random coil. The ability of forming $\beta$-sheets from MAX1I4′ and MAX1I4 was intermediate, but the latter showed a relatively stronger propensity than the former. These changes in secondary structure with respect to different primary structures and time are consistent with the observed changes in rheological data as described above, all showing that the isoleucine substitution for valine favors the formation of $\beta$-sheet structure (self-assembly) and hydrogel formation.

Intermolecular $\beta$-sheet hydrogen bonding promotes the growth of peptide assemblies along the axial direction, thus leading to long fibrils, tubes and ribbons.[51,52] TEM imaging indicated that the four peptides all formed long fibrils at 2 wt %, consistent with their $\beta$-sheet conformation (Figure 6). Furthermore, these peptide fibrils display similar diameters of ~3 nm, consistent with the width of an individual hairpin and the thickness of a hairpin bilayer (Figure 1B). Except for considerable cross-links, they did not show clear signs of

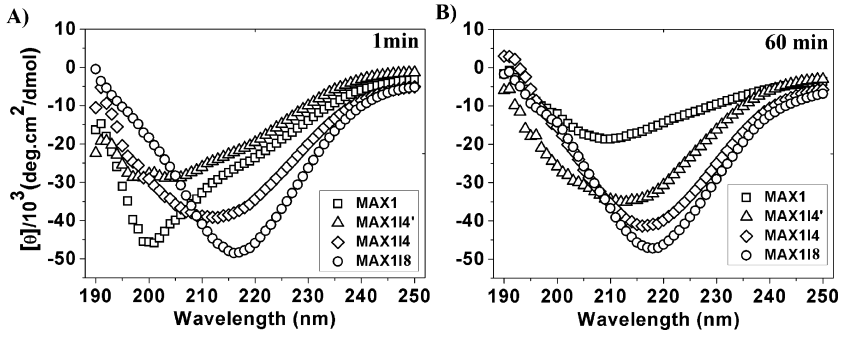


**Figure 5.** CD spectra of 0.5 wt % MAX1, MAX1I4′, MAX1I4, and MAX1I8 at A) 1 min and B) 60 min after adding an equal volume of DMEM (pH 7.4) into peptide solutions in 25 mM Hepes (1 wt %, pH 7.4).


dx.doi.org/10.1021/am5036303 | ACS Appl. Mater. Interfaces 2014, 6, 14360−14368

forming higher-order assemblies such as bundles and laminates. These results thus indicate little impact of the hydrophobic substitutions on the morphology of the fibrils that constitute the gels, in spite of the different propensity in the $\beta$-sheet formation and gelation kinetics caused by the substitutions.

**Cytotoxicity and Biocompatibility of the MAX1I8 Gel.** Pochan and Schneider et al. demonstrated that the MAX1 gel was not cytotoxic toward NIH 3T3 fibroblasts, and the cells showed good attachment and proliferation on the gel surface, similar to those on the control cell culture plate.[50] In spite of the replacement of valines with more hydrophobic isoleucine residues, the resulting MAX1I8 gel also showed a low cytotoxicity. Our MTT assays showed that the MAX1I8 gels induced little changes in $A_{570}$ values over the incubation period (up to 6 days), in comparison with the control TCPS plate (Figure 7A), indicating a similar cellular viability. Furthermore, an increase of $A_{570}$ from ~0.25 at 1 day to ~2.0 at 5 days was indicative of a high level of cell growth and proliferation on both the gels and TCPS surfaces. After incubation for 5 days, $A_{570}$ leveled off, possibly due to the achievement of the full cell confluency. As shown in Figure 7B, inverted light microscopic observations showed good attachment of NIH 3T3 cells. Some of the cells were beginning to adopt spread morphology on the gel surface after incubation for 5 h. Significant cell crowding was observed after 3 days, consistent with the outcome from the MTT assays. Confocal fluorescence microscopy images also indicated good attachment and growth of NIH 3T3 and HEK 293 cells on the gels, which were taken after incubation for 19 h (Figure 7C). Note that cell culture experiments were performed at 37 °C. Such an increase in temperature did not deteriorate the stability of the gel, and, instead, it slightly improved the gel's mechanical stiffness due to the increased hydrophobic interaction (Figure S1).

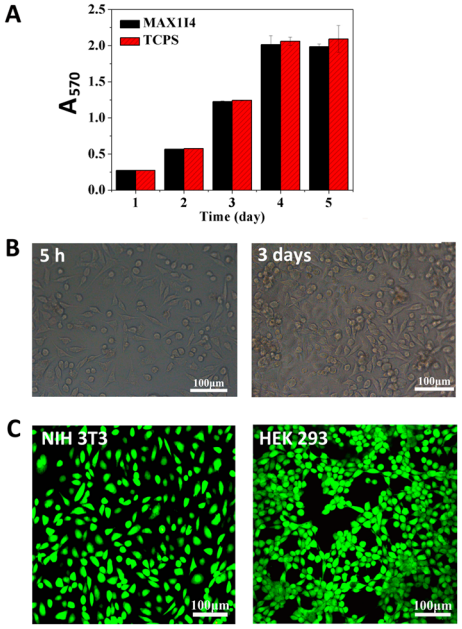


**Figure 7.** A) MTT assay results with NIH 3T3 cells on MAX1I8 gels and TCPS plates. B) Inverted light microscopic images of NIH3T3 cells incubated on the MAX1I8 gel surface for 5 h and 3 days. C) Confocal fluorescence microscopic images of NIH 3T3 cells and HEK293 cells after incubation for 19 h on the MAX1I8 gel surface. Note that the cells were stained with calcein-AM prior to fluorescence microscopic observation.

IL8 and TNF$\alpha$ genes are regarded as the major immune system signaling molecules which can respond to foreign invasions.[53] To assess the inflammatory potential of the MAX1I8 gel, we detected their transcriptional levels of lymphocytes following incubation on the gel surface. As shown in Figure 8A, the lymphocytes on the gel displayed similar transcriptional levels of IL8 and TNF$\alpha$ genes to those incubated on the TCPS plate. As a positive control, LPS (an essential hallmark of the outer membrane of Gram-negative bacteria and elicit strong immune responses in animals) induced high transcriptional levels of IL8 and TNF$\alpha$ genes, which were almost 100 times higher than the amounts detected on the gel surface and the TCPS plate. Furthermore, the cell culture media were analyzed via the ELISA method to quantify the soluble TNF$\alpha$ and IL8 secreted by the lymphocytes after incubation for 48 h.[49] The lymphocytes cultured on the gel surface produced low concentrations of TNF$\alpha$ and IL8 proteins, similar to those in the TCPS wells without the gel. However, the addition of LPS at a concentration of 2 $\mu$g/mL induced significantly elevated secretion of TNF$\alpha$ and IL8, which was about 30 times higher than those secreted by the lymphocytes on the TCPS plate or MAX1I8 hydrogel (Figure 8B). The results indicate that MAX1I8 hydrogel cannot induce nonspecific immunogenic responses, suggesting its good biocompatibility. The low cytotoxicity and good biocompatibility of MAX1I8 are reminiscent of antibacterial and anticancer $G(IIKK)_{2-4}I\text{-}NH_2$ peptides. The peptides designed by us with a similar amino acid composition tend to form $\alpha$-helical structures due to the lack of a hairpin motif.[47,54] Furthermore, they also show low cytotoxicity toward normal cells and do not induce nonspecific immunological effects when killing bacterial and cancer cells.

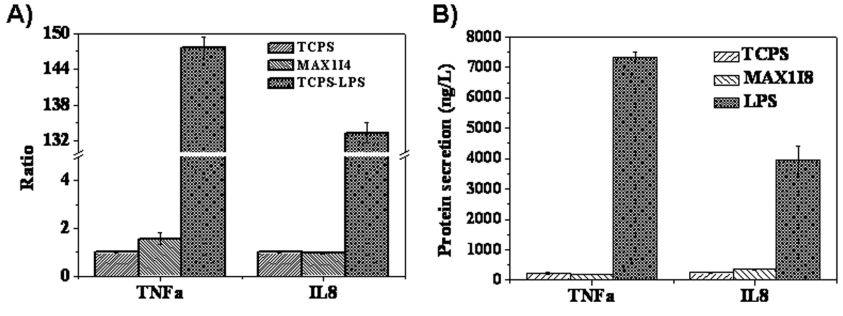


**Figure 8.** TNF$\alpha$ and IL8 A) gene transcription levels and B) protein secretion concentrations of lymphocytes following their incubation on the MAX1I8 gel surface as well as the TCPS wells without the gel in the absence or presence of 2 $\mu$g/mL LPS.

**Cell Distribution within 3D Gels.** Figure 9 shows cell distributions in 2 wt % MAX1 and MAX1I8 solutions at 5 and 30 min after their hydrogelation processes were triggered through the addition of DMEM containing prestained NIH 3T3 cells. At 5 min, NIH 3T3 cells were almost homogeneously distributed within the two solutions. At 30 min, the cell distribution did not change in the case of MAX1I8, while cells mostly deposited to the bottom of the field for MAX1. This can be interpreted as the difference in their hydrogelation kinetics and the lack of sufficient mechanical strength to sustain the cell bodies within the 3D gel network. As indicated above, 2 wt % MAX1I8 can attain a $G'$ of 100 Pa within the first 30 s, thus affording a rigid support for the 3D cell distribution. In contrast, 2 wt % MAX1 required about 75 min to attain a $G'$ of 100 Pa. Note that while the cell encapsulation had little effect on the hydrogelation processes, the lack of gel rigidity or strength in the case of MAX1 led to the apparent cell precipitation.

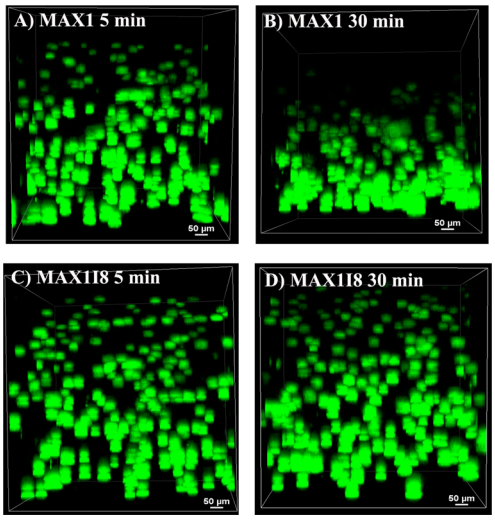


**Figure 9.** 3D confocal microscopic images showing the cell distributions within 2 wt % MAX1 and MAX1I8 at room temperature with time: A) and C) 5 min and B) and D) 30 min. Note that the cells were prelabeled with Calcein-AM. Scale bar = 50 $\mu$m. The width, height, and depth of the images fields are 1.27, 1.27, and 1.27 mm, respectively.

## 4. DISCUSSION

For MAX1 and its derivatives, Pochan and Schneider et al. indicated that their hydrogelation was realized via an identical pathway. Intramolecular folding produces a hairpin structure that is facially amphiphilic, and the consequent self-assembly of numerous hairpins leads to the formation of nanofibrils, driven by the combination of lateral intermolecular hydrogen bonding and facial hydrophobic collapse.[30,32,35−39,41−44,50] After substituting valine residues with isoleucines, the resulting MAX1I4′, MAX1I4, and MAX1I8 follow the same hydrogelation pathway (Figure 1B), leading to the networks of fibrils rich in $\beta$-sheet and with the diameters of ∼3 nm that are close to both the width of an individual hairpin (3.2 nm) and the thickness of a bilayer of hairpins (2.5 nm). However, due to the higher hydrophobicity and the stronger propensity for $\beta$-sheet structuring of isoleucine,[45,46] its substitution for valine favors intramolecular folding and intermolecular interactions (hydrogen bonding and hydrophobic interaction), leading to faster self-assembly and hydrogelation rates as well as enhancing the resulting gel rigidity (Figures 2 and 3). These improvements were found to be dependent not only on the number of residue substitutions but also on the substitution positions. Thus, the MAX1I4 gel exhibited a faster gelation rate and a higher mechanical stiffness than the MAX1I4′ gel. The MAX1I8 with all eight valines replaced with isoleucines showed the fastest hydrogelation kinetics (gelation within 5 min) due to increased hydrogen bonding and hydrophobic interaction and formed gels with the highest rigidity within the series. Such a fast gelation rate allows an almost uniform cell distribution within the resulting 3D scaffold, and this was achieved simply by mixing DMEM containing cells with the MAX1I8 solution (Figure 7). This feature of the MAX1I8 gel benefits its practical applications as regenerative scaffolds and delivery vesicles, in which uniform cell/drug density is an important requirement for reproducible control. With this kind of $\beta$-hairpin peptide, another strategy for increasing hydrogelation kinetics is substitution for a positively charged lysine residue with a negatively charged glutamic acid.[30] The resulting peptide ($VKVKVKVKV^{D}PPTKVEVKVKV\text{-}NH_2$) also showed faster self-assembly and hydrogelation rates because its net positive charge was lowered by 2.

The MAX1I8 gel also showed shear-thinning and rapid recovery upon cessation of shear, and, since only some of the physical connections are disrupted by shear, the gel recovers at a faster rate than the initial hydrogelation (Figure 4). The shear-thinning property will allow the preformed gel containing cells or drugs to be injected as a flowing liquid to a target site. Once the injection shear is stopped, the rapid recovery will enable the gel and its encapsulations to remain localized at the target site.

Finally, the MAX1I8 gel showed low cytotoxicity and good biocompatibility. Although isoleucine has a higher hydrophobicity, its substitution for valine did not induce higher toxicity against normal cells and nonspecific immunological effects. In general, for self-assembling $\beta$-sheet peptides, isoleucine is an ideal constituent due to its high hydrophobicity and strong promotion of $\beta$-sheet formation. Thus, we have recently designed the ultrashort peptide $I_3K$, which can readily self-assemble into long and stable fibrils,[51] whereas the similar $L_3K$ can only self-assemble into spherical stacks rather than long fibrils because it lacks the same propensity for $\beta$-sheet formation.

## 5. CONCLUSIONS

This study demonstrates that gelation kinetics and mechanical rigidity of self-assembling $\beta$-hairpin peptide hydrogels can be tuned by residue substitution. Because isoleucine has higher hydrophobicity and the stronger propensity for $\beta$-sheet structuring than valine, its substitution for the valine residues of MAX1 leads to faster self-assembly, hydrogelation kinetics, and higher gel rigidity. These improvements are dependent on not only the number of residue substitutions but also on the substitution positions. The MAX1I8 with all eight valine resdiues replaced with isoleucines showed the fastest hydrogelation rate and formed gels with the highest rigidity in the investigated peptide series, thus allowing a nearly uniform cell distribution within the resulting 3D scaffold. In addition, the MAX1I8 gel showed rapid shear-thinning and recovery rates, low cytotoxicity, and good biocompatibility, indicating great potential for developing it as cell culture and delivery scaffolds. Further effort will focus on the *in vivo* biochemical character-

izations of the gel and its applications under conditions close to clinical uses.

## ■ ASSOCIATED CONTENT

### Supporting Information

The evolution of storage moduli ($G'$) of the MAX1I8 hydrogel (2 wt %) with time at 25 and 37 °C and the photograph of the gel on a vertical glass surface after syringe delivery. This material is available free of charge via the Internet at http://pubs.acs.org.

## ■ AUTHOR INFORMATION

### Corresponding Author

*Phone: 86-532-86981569. E-mail: xuh@upc.edu.cn.

### Notes

The authors declare no competing financial interest.

## ■ ACKNOWLEDGMENTS

We thank Dr Robert Thomas (University of Oxford) for helpful discussions and commentary on the manuscript. This work was supported by the National Natural Science Foundation of China under grant numbers 21373270 and 31271497, the Natural Science Foundation of Shandong Province (ZR2009DQ001 and JQ201105), and the Fundamental Research Funds for the Central Universities (12CX04052A and 14CX02189A).

## ■ REFERENCES

(1) Whitesides, G. M.; Grzybowski, B. Self-Assembly at All Scales. *Science* **2002**, *295*, 2418−2421.
(2) Zhang, S. Fabrication of Novel Biomaterials through Molecular Self-Assembly. *Nat. Biotechnol.* **2003**, *215*, 1171−1178.
(3) Holmes, T. C.; de Lacalle, S.; Su, X.; Liu, G.; Rich, A.; Zhang, S. Extensive Neurite Outgrowth and Active Synapse Formation on Self-Assembling Peptide Scaffolds. *Proc. Natl. Acad. Sci. U. S. A.* **2000**, *97*, 6728−6733.
(4) Kisiday, J.; Jin, M.; Kurz, B.; Hung, H.; Semino, C.; Zhang, S.; Grodzinsky, A. J. Self-Assembling Peptide Hydrogel Fosters Chondrocyte Extracellular Matrix Production and Cell Division: Implications for Cartilage Tissue Repair. *Proc. Natl. Acad. Sci. U. S. A.* **2002**, *99*, 9996−10001.
(5) Silva, G. A.; Czeisler, C.; Niece, K. L.; Beniash, E.; Harrington, D. A.; Kessler, J. A.; Stupp, S. I. Selective Differentiation of Neural Progenitor Cells by High-Epitope Density Nanofibers. *Science* **2004**, *303*, 1352−1355.
(6) Kiley, P.; Zhao, X.; Vaughn, M.; Baldo, M. A.; Bruce, B. D.; Zhang, S. Self-Assembling Peptide Detergents Stabilize Isolated Photosystem I on a Dry Surface for an Extended Time. *PLoS Biol.* **2005**, *3*, e230.
(7) Davis, M. E.; Motion, J. P. M.; Narmoneva, D. A.; Takashi, T.; Hakuno, D.; Kamm, R. D.; Zhang, S.; Lee, R. T. Injectable Self-Assembling Peptide Nanofibers Create Intramyocardial Microenvironments for Endothelial Cells. *Circulation* **2005**, *111*, 442−450.
(8) Ellis-Behnke, R. G.; Liang, Y. X.; You, S. W.; Tay, D. K. C.; Zhang, S.; So, K. F.; Schneider, G. E. Nano Neuro Knitting: Peptide Nanofiber Scaffold for Brain Repair and Axon Regeneration with Functional Return of Vision. *Proc. Natl. Acad. Sci. U. S. A.* **2006**, *103*, 5054−5059.
(9) Horii, A.; Wang, X.; Gelain, F.; Zhang, S. Biological Designer Self-Assembling Peptide Nanofiber Scaffolds Significantly Enhance Osteoblast Proliferation, Differentiation and 3-D Migration. *PLoS One* **2007**, *2*, e190.
(10) Schneider, A.; Garlick, J. A.; Egles, C. Self-Assembling Peptide Nanofiber Scaffolds Accelerate Wound Healing. *PLoS One* **2008**, *1*, e1410.
(11) Zhou, M.; Smith, A. M.; Das, A. K.; Hodson, N. W.; Collins, R. F.; Ulijn, R. V.; Gough, J. E. Self-Assembled Peptide-Based Hydrogels as Scaffolds for Anchorage-Dependent Cells. *Biomaterials* **2009**, *30*, 2523−2530.
(12) Branco, M. C.; Pochan, D. J.; Wagner, N. J.; Schneider, J. P. Macromolecular Diffusion and Release from Self-Assembled $\beta$-Hairpin Peptide Hydrogels. *Biomaterials* **2009**, *30*, 1339−1347.
(13) Salick, D. A.; Pochan, D. J.; Schneider, J. P. Design of an Injectable $\beta$-Hairpin Peptide Hydrogel that Kills Methicillin-Resistant *Staphylococcus Aureus*. *Adv. Mater.* **2009**, *21*, 4120−4123.
(14) Standley, S. M.; Toft, D. J.; Cheng, H.; Soukasene, S.; Chen, J.; Raja, S. M.; Band, V.; Band, H.; Cryns, V. L.; Stupp, S. I. Induction of Cancer Cells Death by Self-Assembling Nanostructures Incorporation a Cytotoxic Peptide. *Cancer Res.* **2010**, *70*, 3020−3026.
(15) Chen, C.; Pan, F.; Zhang, S.; Hu, J.; Cao, M.; Wang, J.; Xu, H.; Zhao, X.; Lu, J. R. Antibacterial Activities of Short Designer Peptides: a Link between Propensity for Nanostructuring and Capacity for Membrane Destabilization. *Biomacromolecules* **2010**, *11*, 402−411.
(16) Altunbas, A.; Lee, S. J.; Rajasekaran, S. A.; Schneider, J. P.; Pochan, D. J. Encapsulation of Curcumin in Self-Assembling Peptide Hydrogels as Injectable Drug Delivery Vehicles. *Biomaterials* **2011**, *32*, 5906−5914.
(17) Luo, Z.; Wang, S.; Zhang, S. Fabrication of Self-Assembling D-Form Peptide Nanofiber Scaffold d-EAK16 for Rapid Hemostasis. *Biomaterials* **2011**, *32*, 2013−2020.
(18) Bakota, E.; Wang, Y.; Danesh, F. R.; Hartgerink, J. D. Injectable Multidomain Peptide Nanofiber Hydrogel as a Delivery Agent for Stem Cell Secretome. *Biomacromolecules* **2011**, *12*, 1651−1657.
(19) Xu, H.; Chen, C.; Hu, J.; Zhou, P.; Zeng, P.; Cao, C.; Lu, J. R. Dual Modes of Antitumor Action of an Amphiphilic Peptide $A_9K$. *Biomaterials* **2013**, *34*, 2731−2737.
(20) Zheng, W.; Gao, J.; Song, L.; Chen, C.; Guan, D.; Wang, Z.; Li, Z.; Kong, D.; Yang, Z. Surface-Induced Hydrogelation Inhibits Platelet Aggregation. *J. Am. Chem. Soc.* **2013**, *135*, 266−271.
(21) Jung, J. P.; Gasiorowski, J. Z.; Collier, J. H. Fibrillar Peptide Gels in Biotechnology and Biomedicine. *Biopolymers* **2010**, *94*, 49−59.
(22) Collier, J. H.; Rudra, J. S.; Gasiorowski, J. Z.; Jung, J. P. Multi-Component Extracellular Matrices Based on Pepide Self-Assembly. *Chem. Soc. Rev.* **2010**, *39*, 3413−3424.
(23) Yan, C.; Pochan, D. J. Rheological Properties of Peptide-Based Hydrogels for Biomedical and Other Applications. *Chem. Soc. Rev.* **2010**, *39*, 3528−3540.
(24) Matson, J. B.; Stupp, S. I. Self-Assembling Peptide Scaffolds for Regenerative Medicine. *Chem. Commun.* **2012**, *48*, 26−33.
(25) Wu, E. C.; Zhang, S.; Hauser, C. A. Self-Assembling Peptides as Cell-Interactive Scaffolds. *Adv. Funct. Mater.* **2012**, *22*, 456−68.
(26) Levental, I.; Georges, P. C.; Janmey, P. A. Soft Biological Materials and Their Impact on Cell Function. *Soft Matter.* **2007**, *3*, 299−306.
(27) Discher, D. E.; Janmey, P.; Wang, Y. L. Tissue Cells Feel and Respond to the Stiffness of Their Substrate. *Science* **2005**, *310*, 1139−1143.
(28) Georges, P. C.; Janmey, P. A. Cell Type-Specific Response to Growth on Soft Materials. *J. Appl. Physiol.* **2005**, *98*, 1547−1153.
(29) Pelham, R. J.; Wang, Y. L. Cell Locomotion and Focal Adhesions are Regulated by Substrate Flexibility. *Proc. Natl. Acad. Sci. U. S. A.* **1997**, *94*, 13661−13665.
(30) Haines-Butterick, L.; Rajagopal, K.; Branco, M.; Salick, D.; Rughani, R.; Pilarz, M.; Lamm, M. S.; Pochan, D. J.; Schneider, J. P. Controlling Hydrogelation Kinetics by Peptide Design for Three-Dimensional Encapsulation and Injectable Delivery of Cells. *Proc. Natl. Acad. Sci. U. S. A.* **2007**, *104*, 7791−7796.
(31) Jung, J. P.; Jones, J. L.; Cronier, S. A.; Collier, J. H. Modulating the Mechanical Properties of Self-Assembled Peptide Hydrogels via Native Chemical Ligation. *Biomaterials* **2008**, *29*, 2143−2151.
(32) Aulisa, L.; Dong, H.; Hartgerink, J. D. Self-Assembly of Multidomain Peptides: Sequence Variation Allows Control over Cross-Linking and Viscoelasticity. *Biomacromolecules* **2009**, *10*, 2694−2698.

(33) Cao, C.; Cao, M.; Fan, H.; Xia, D.; Xu, H.; Lu, J. R. Redox Modulated Hydrogelation of a Self-Assembling Short Peptide Amphiphile. *Chin. Sci. Bull.* **2012**, *57*, 4296−4303.
(34) Bakota, E. L.; Aulisa, L.; Galler, K. M.; Hartgerink, J. D. Enzymatic Cross-Linking of a Nanofibrous Peptide Hydrogel. *Biomacromolecules* **2011**, *12*, 82−87.
(35) Ozbas, B.; Rajagopal, K.; Haines-Butterick, L.; Schneider, J. P.; Pochan, D. J. Reversible Stiffening Transition in $\beta$-Hairpin Hydrogels Induced by Ion Complexation. *J. Phys. Chem. B* **2007**, *111*, 13901−13908.
(36) Micklithsch, C. M.; Kner, P. J.; Branco, M. C.; Nagarkar, R.; Pochan, D. J.; Schneider, J. P. Zinc-Triggered Hydrogelation of a Self-Assembling $\beta$-Hairpin Peptide. *Angew. Chem. Ind. Ed.* **2011**, *50*, 1577−1579.
(37) Nagy, K. J.; Giano, M. C.; Jin, A.; Pochan, D. J.; Schneider, J. P. Enhanced Mechanical Rigidity of Hydrogels Formed from Enantiomeric Peptide Assemblies. *J. Am. Chem. Soc.* **2011**, *133*, 14975−14957.
(38) Rajagopal, K.; Lamm, M. S.; Haines-Butterick, L. A.; Pochan, D. J.; Schneider, J. P. Tuning the pH Responsiveness of $\beta$-Hairpin Peptide Folding, Self-Assembly, and Hydrogel Material Formation. *Biomacromolecules* **2009**, *10*, 2619−2625.
(39) Larsen, T. H.; Branco, M. C.; Rajagopal, K.; Schneider, J. P.; Furst, E. M. Sequence-Dependent Gelation Kinetics of $\beta$-Hairpin Peptide Hydrogels. *Macromolecules* **2009**, *42*, 8443−8450.
(40) Bowerman, C. J.; Liyanage, W.; Federation, A. J.; Nilsson, B. Tuning $\beta$-Sheet Peptide Self-Assembly and Hydrogelation Behavior by Modification of Sequence Hydrophobicity and Aromaticity. *Biomacromolecules* **2011**, *12*, 2735−2745.
(41) Schneider, J. P.; Pochan, D. J.; Ozbas, B.; Rajagopal, K.; Pakstis, L.; Kretsinger, J. Responsive Hydrogels from the Intramolecular Folding and Self-Assembly of a Designed Peptide. *J. Am. Chem. Soc.* **2002**, *124*, 15030−15037.
(42) Ozbas, B.; Kretsinger, J.; Rajagopal, K.; Schneider, J. P.; Pochan, D. J. Salt-Triggered Peptide Folding and Consequent Self-Assembly into Hydrogels with Tunable Modulus. *Macromolecules* **2004**, *37*, 7331−7337.
(43) Pochan, D. J.; Schneider, J. P.; Krestsinger, J.; Ozbas, B.; Rajagopal, K.; Haines, L. Thermally Reversible Hydrogels via Intramolecular Folding and Consequent Self-Assembly of a *de novo* Designed Peptide. *J. Am. Chem. Soc.* **2003**, *125*, 11802−11803.
(44) Rajagopal, K.; Ozbas, B.; Pochan, D. J.; Schneider, J. P. Probing the Importance of Lateral Hydrophobic Association in Self-Assembling Peptide Hydrogelators. *Eur. Biophys. J.* **2006**, *35*, 162−169.
(45) Monera, O. D.; Sereda, T. J.; Zhou, N. E.; Kay, C. M.; Hodges, R. S. Relationship of Sidechain Hydrophobicity and $\alpha$-Helical Propensity on the Stability of the Single-Stranded Amphipathic $\alpha$-Helix. *J. Pept. Sci.* **1995**, *1*, 319−329.
(46) Daniel, L.; Minor, J.; Kim, P. S. Measurement of the $\beta$-Sheet-Forming Propensities of Amino Acids. *Nature* **1994**, *367*, 660−663.
(47) Chen, C.; Hu, J.; Zeng, P.; Pan, F.; Yaseen, M.; Xu, H.; Lu, J. R. Molecular Mechanisms of Anticancer Action and Cell Selectivity of Short $\alpha$-Helical Peptides. *Biomaterials* **2014**, *35*, 1552−1561.
(48) Livak, K. J.; Schmittgen, T. D. Analysis of Relative Gene Expression Data using Real-Time Quantitative PCR and the $2^{-\Delta\Delta Ct}$ Method. *Methods* **2001**, *25*, 402−408.
(49) Haines-Butterick, L. A.; Salick, D. A.; Pochan, D. J.; Schneider, J. P. *In vitro* Assessment of the Pro-Inflammatory Potential of $\beta$-Hairpin Peptide Hydrogels. *Biomaterials* **2008**, *29*, 4164−4169.
(50) Kretsinger, J. K.; Haines, L. A.; Ozbas, B.; Pochan, D. J.; Schneider, J. P. Cytocompatibility of Self-Assembled $\beta$-Hairpin Peptide Hydrogel Surfaces. *Biomaterials* **2005**, *26*, 5177−5186.
(51) Han, S.; Cao, S.; Wang, Y.; Wang, J.; Xia, D.; Xu, H.; Zhao, X.; Lu, J. R. Self-Assembly of Short Peptide Amphiphiles: the Cooperative Effect of Hydrophobic Interaction and Hydrogen Bonding. *Chem.—Eur. J.* **2011**, *17*, 13095−13102.
(52) Zhao, Y.; Wang, J.; Deng, L.; Zhou, P.; Wang, S.; Wang, Y.; Xu, H.; Lu, J. R. Tuning the Self-Assembly of Short Peptides via Sequence Variations. *Langmuir* **2013**, *29*, 13457−13464.
(53) De, G. D.; Zangerle, P. F.; Gevaert, Y.; Fassotte, M. F.; Beguin, Y.; Noizat-Pirenne, F.; Pirenne, J.; Gathy, R.; Lopez, M.; Dehart, I.; Igot, D.; Baudrihaye, M.; Delacroix, D.; Franchimont, P. Direct Stimulation of Cytokines (IL-1$\beta$, TNF-$\alpha$, IL-6, IL-2, IFN-$\gamma$ and GM-CSF) in Whole Blood. I. Comparison with Isolated PBMC Stimulation. *Cytokines* **1992**, *4*, 239−248.
(54) Hu, J.; Chen, C.; Zhang, S.; Xu, H.; Zhao, X.; Lu, J. R. Designed Antimicrobial and Antitumor Peptides with High Selectivity. *Biomacromolecules* **2011**, *12*, 3839−3843.